

Confined thermocapillary motion of a three-dimensional deformable drop

P. T. Brady,¹ M. Herrmann,¹ and J. M. Lopez^{2,a)}

¹*School for Engineering of Matter, Transport and Energy, Arizona State University, Tempe, Arizona 85287, USA*

²*School of Mathematical and Statistical Sciences, Arizona State University, Tempe, Arizona 85287, USA*

(Received 1 July 2010; accepted 28 November 2010; published online 3 February 2011)

In this paper, simulations are performed of the thermocapillary motion of three-dimensional and axisymmetric drops in a confined apparatus. The refined level-set grid method is used to track the interface and resolve very small deformations. We compare our results to theoretically predicted thermocapillary migration velocities of drops and to experimentally measured migration velocities in microgravity experiments. The motivation of the present work is to address four important questions surrounding thermocapillary migration. These are as follows. (1) What is the impact of initial conditions on both the initial transient and steady state drop behavior? (2) What is the impact of the domain geometry on drop behavior? (3) Do drops deform for intermediate Marangoni numbers and are those deformations axisymmetric? (4) Can the assumption of constant temperature fluid properties be used when simulating physical experiments? To answer the first question, we explore the parameter space of initial drop temperature distribution and drop holding time. We find that in lower Marangoni number regimes, the drop rapidly settles to a quasisteady state. For larger Marangoni numbers, the initial conditions dominate the drop behavior. To address the second and third questions, we look at the spatial distribution of tangential temperature gradients on the surface of the drop as well as drop deformations and migration velocities. The domain geometry induces nonaxisymmetric deformations and temperature distributions. The results of several axisymmetric runs with realistic physical properties are examined to answer the fourth question. It is found that the variation of material properties influences the drop migration behavior in a nontrivial way.

© 2011 American Institute of Physics. [doi:10.1063/1.3529442]

I. INTRODUCTION

Thermal fluctuations can have a significant impact on the dynamics of gas/liquid interfaces, because for most gas/liquid combinations both surface tension and phase transition depend strongly on the local temperature. Important technical applications where this is the case include the atomization of liquid fuels for combustion processes and flows of bubbles and drops in zero-gravity environments.

A canonical multiphase flow problem isolating the impact of nonisothermal flows is the thermal Marangoni-driven migration of drops and bubbles. The first reported study of the thermocapillary motion determined the terminal velocity of an unconfined spherical drop in the creeping flow limit.¹ Under those conditions, the drop does not deform and a steady migration is achieved in an environment with a linear temperature profile. There have been numerous subsequent studies relaxing the creeping flow limit, but for the most part these have neglected any deformations of the drop (see review articles^{2,3}). The main motivation for those studies stems from microgravity applications in which the velocities involved may be small enough to justify neglecting deformations; however, this is not generally the case.

The first numerical study of surface deformations of an axisymmetric bubble due to thermocapillary motion showed that deformations tend to reduce the bubble's velocity.⁴ The

first three-dimensional computations of the thermocapillary motion of deforming drops or bubbles found, for the parameter regimes considered, that the drops or bubbles remain axisymmetric, but deform into either oblate or prolate spheroids depending on the density ratio between the drop/bubble and the bulk.⁵ Their numerical results were consistent with earlier predictions from axisymmetric analysis in the limit of large thermal diffusivity.⁶ In an axisymmetric numerical study of a deforming bubble with larger inertia,⁷ it was found that not only does the velocity of the bubble reduce due to deformations, but that for large enough inertia the bubble does not settle to a steady migration velocity. The study of thermocapillary motion in systems with several drops was first studied in the limit of zero inertia,⁸ showing that in the creeping flow limit the drops do not interact. More recently, inertial effects have been included and strong interactions between the deformable three-dimensional drops have been reported.^{9,10}

Studies of a single drop with nonzero inertia allowing for fully three-dimensional deformations are very scarce; we are only aware of one study.⁵ Very recently, diffuse-interface models using a phase-field approach have been reported¹¹ which account for a temperature-dependent generalized surface tension (in the phase-field sense), but the numerical results were restricted to planar two-dimensional flows.

Experimental investigations of the thermocapillary motion of drops and bubbles are hampered by gravitational effects which tend to mask the thermocapillary effect, unless

^{a)}Author to whom correspondence should be addressed. Electronic mail: lopez@math.asu.edu.

they are conducted in a low-gravity environment. A number of experiments have been conducted in drop towers, sounding rockets, and aboard space shuttles; see the extensive review article.³ Some of the more recent experiments motivate our present investigation. These experiments have noted complicated transients and time-dependent behavior in regimes where the flow has finite viscous and thermal inertia.^{12–14} Those experimental studies noted that there are no theoretical or numerical results with which to compare their experiments.

For a viscous drop there are four time scales which come into play in determining the transient evolution: r_0^2/ν_d , r_0^2/ν_b , r_0^2/α_d , and r_0^2/α_b , where r_0 is the drop radius, ν is the kinematic viscosity, α is the thermal diffusivity, and the subscripts d and b refer to the drop and bulk liquids, respectively. In the microgravity experiments these time scales differ by up to two orders of magnitude within a single experimental run, and so complicated temporal behavior is not surprising. The experiments in the drop tower,¹² having the relative luxury of being able to repeat many experimental runs under nominally the same conditions, noted that the problem is very sensitive to initial conditions. It has also been noted by several investigators that in the experiments it has not been possible to determine the initial temperature distribution inside the drop. A recent numerical study with nondeforming spherical bubbles noted that the early transients are very sensitive to the initial temperature distribution.¹⁵ Furthermore, the liquids used in the experiments (silicone oils for the bulk phase) have temperature-dependent viscosity and density, and for the temperature gradients used these variations are nontrivial. All of the presently available theoretical and numerical results assume constant fluid properties, except for the surface tension which is assumed to vary linearly with temperature. The review article³ concluded that the most important theoretical problem that needs to be addressed for an isolated drop is the consideration of the fully transient problem accommodating the dependence of physical properties on temperature.

In this paper, we aim to answer four open questions associated with experimental results of single drop thermocapillary migration in microgravity.³ (i) What is the impact of the initial temperature distribution inside the drop on the transient motion of the drop? (ii) What is the impact of using a square box geometry^{13,14} in an otherwise axisymmetric problem? (iii) Do drops deform for intermediate Marangoni numbers and are those deformations axisymmetric? (iv) Does the temperature dependence of density and viscosity of the two fluids impact the transient motion?

II. GOVERNING EQUATIONS

Consider a spherical drop of one fluid with radius r_0 placed in an initially quiescent bulk fluid with an imposed (typically positive) constant temperature gradient G_T in the vertical direction. In general, the two fluids are immiscible with different densities, viscosities, and thermal properties. We shall assume that the surface tension σ^* between the two fluids varies linearly with gradient σ_T (which for most fluids of interest is negative),

$$\sigma^*(T^*) = \sigma_0 + \sigma_T(T^* - T_0^*), \quad (1)$$

where σ_0 is the surface tension at some suitable reference temperature T_0^* .

We shall use the initial radius of the drop r_0 as the length scale and $G_T r_0$ as the temperature scale. For the thermocapillary motion of drops and bubbles, it is customary to use $U = \sigma_T G_T r_0 / \mu_b$ as the velocity scale, where μ_b is the dynamic viscosity of the bulk phase. This then gives $\mu_b / \sigma_T G_T$ as the time scale. The surface tension is scaled by σ_0 , which for the problems considered here is the surface tension at the initial temperature at the center of the drop. Throughout, subscript d refers to properties of the drop phase and subscript b to those of the bulk phase.

With these scalings, the nondimensional linear equation of state becomes

$$\sigma(T) = 1 + \text{Ca}(T - T_0), \quad (2)$$

where T_0 is the nondimensional initial temperature at the center of the drop, and the capillary number, which gives the relative importance of the tangential to normal stresses at the drop interface, is

$$\text{Ca} = \frac{\mu_b U}{\sigma_0} = \frac{\sigma_T G_T r_0}{\sigma_0}. \quad (3)$$

The nondimensional Navier–Stokes equations governing the motion of an unsteady, incompressible, immiscible two-fluid system are

$$\begin{aligned} \rho_r \left(\frac{\partial \mathbf{u}}{\partial t} + \mathbf{u} \cdot \nabla \mathbf{u} \right) \\ = -\nabla P + \frac{1}{\text{Re}} \nabla \cdot \mu_r (\nabla \mathbf{u} + \nabla^T \mathbf{u}) + \frac{1}{\text{We}} \mathbf{F} - \frac{\rho_r}{\text{Fr}} \hat{\mathbf{z}}, \end{aligned} \quad (4)$$

$$\nabla \cdot \mathbf{u} = 0, \quad (5)$$

where \mathbf{u} is the nondimensional velocity, P the nondimensional pressure, the relative dynamic viscosity $\mu_r = 1$ in the bulk phase and $\mu_r = \mu_d / \mu_b$ in the drop phase, and the relative density $\rho_r = 1$ in the bulk phase and $\rho_r = \rho_d / \rho_b$ in the drop phase. The Weber number is

$$\text{We} = \text{Re} \text{Ca} = \frac{\rho_b r_0 U^2}{\sigma_0}. \quad (6)$$

The Froude number is

$$\text{Fr} = U^2 / g r_0 = \frac{(\sigma_T G_T r_0)^2}{\mu_b^2 g r_0}, \quad (7)$$

where g is the gravitational acceleration and $\hat{\mathbf{z}}$ is a unit vector in the z direction. In this paper, we consider the limit of zero gravity for which $\text{Fr} \rightarrow \infty$.

The (dimensional) surface force \mathbf{F}^* , which is nonzero only at the location of the drop interface \mathbf{x}_f , is¹⁶

$$\mathbf{F}^*(\mathbf{x}) = \sigma^*(T^*) \kappa^* \delta^* \mathbf{n} + \nabla_{\parallel} \sigma^*(T^*) \delta^*, \quad (8)$$

where \mathbf{n} is the local drop interface normal and δ^* the interface delta function. Nondimensionalizing with the above scalings, and substituting the linear equation of state for the surface tension, the nondimensional surface force is

$$\frac{\text{Re}}{\text{We}} \mathbf{F} = \kappa \frac{\delta \mathbf{n}}{\text{Ca}} + \kappa(T - T_0) \delta \mathbf{n} + \nabla_{\parallel} T \delta, \quad (9)$$

where κ is the local interface curvature and ∇_{\parallel} is the tangential surface derivative. The first two terms on the right-hand side correspond to the isothermal normal stress balance and the temperature-dependent normal stress balance, and the third term corresponds to the Marangoni force.

The nondimensional heat equation for the temperature is

$$\rho_r c_{p_r} \left(\frac{\partial T}{\partial t} + \nabla \cdot (T \mathbf{u}) \right) = \frac{1}{\text{Ma}} \nabla \cdot (k_r \nabla T), \quad (10)$$

where the relative thermal conductivity $k_r=1$ in the bulk phase and $k_r=k_d/k_b$ in the drop, the relative specific heat $c_{p_r}=1$ in the bulk phase and $c_{p_r}=c_{p_d}/c_{p_b}$ in the drop. The thermal conductivity k is related to the thermal diffusivity α by $\alpha=k/\rho c_p$. The Marangoni number is

$$\text{Ma} = \frac{U r_0 \rho_b c_{p_b}}{k_b} = \frac{U r_0}{\alpha_b} = \frac{\sigma_T G_T r_0^2}{\mu_b \alpha_b} = \text{Re Pr}, \quad (11)$$

where the Prandtl number

$$\text{Pr} = \nu_b / \alpha_b \quad (12)$$

is the ratio of viscous to thermal diffusivity in the bulk phase. Note that the Marangoni number is equivalent to the Péclet number, Pe , for the characteristic velocity that is used in the thermocapillary migration of drops or bubbles.

We see that this simple problem of a single drop in a temperature gradient field is governed by several parameters. There are three parameters describing the dynamics: Re , Ca , and Ma (the other three, We , Pe , and Pr , are dependent on these), three ratios of the material properties in the two phases: ρ_r , α_r , and μ_r , as well as a geometric parameter L giving the ratio of the length scale of the environment to the initial radius of the drop.

A. Numerics

To determine the location \mathbf{x}_f of the phase interface, we employ a level-set approach by defining the level-set scalar at the interface $G(\mathbf{x}_f, t)=0$, with $G(\mathbf{x}, t)>0$ in the drop and $G(\mathbf{x}, t)<0$ in the bulk phase. Differentiating this with respect to time yields the level-set equation,

$$\frac{\partial G}{\partial t} + \mathbf{u} \cdot \nabla G = 0. \quad (13)$$

We solve and evaluate all level-set related equations following the refined level-set grid (RLSG) method in a separate level-set solver LIT (Ref. 17) using an auxiliary high-resolution G -grid with a fifth-order WENO scheme¹⁸ in conjunction with a third-order TVD Runge–Kutta time discretization.¹⁹ The phase interface curvature κ is evaluated on the G -grid using a second-order-accurate interface projection method.¹⁷

The balanced-force algorithm for finite-volume solvers¹⁷ is used to solve Eqs. (4) and (5). The algorithm has been implemented in the flow solver NGA,²⁰ which solves the Navier–Stokes equations on a staggered grid using a second-order-accurate fractional step method. A third-order bounded

QUICK scheme is used to solve the temperature equation.²¹ Material properties of the two fluids in each control volume are evaluated by

$$\rho_r = \rho_d / \rho_b \psi_{cv} + (1 - \psi_{cv}), \quad (14)$$

$$\mu_r = \mu_d / \mu_b \psi_{cv} + (1 - \psi_{cv}), \quad (15)$$

where ψ_{cv} is the drop phase volume fraction of a control volume,

$$\psi_{cv} = 1/V_{cv} \int_{V_{cv}} H(G) dV, \quad (16)$$

with V_{cv} the volume of the control volume cv . Equation (16) is evaluated on the fine G -grid using an algebraic expression.²²

The surface force, Eq. (9), needs to be evaluated at the cell faces in the staggered grid layout used here. Its normal component is calculated following the continuum surface force model²³ approximating $\delta \mathbf{n}$ by $\delta \mathbf{n} = \nabla \psi_{cv}$. The tangential derivative of the temperature is calculated by

$$\nabla_{\parallel} T = \nabla T - (\nabla T \cdot \mathbf{n}) \mathbf{n}, \quad (17)$$

where the phase interface normal vector \mathbf{n} is evaluated on the flow solver grid by

$$\mathbf{n} = \frac{\nabla \psi_{cv}}{|\nabla \psi_{cv}|}. \quad (18)$$

This results in the surface force being calculated by

$$\frac{\text{Re}}{\text{We}} \mathbf{F} = \kappa \frac{\nabla \psi}{\text{Ca}} + \kappa(T - T_0) \nabla \psi + \nabla T |\nabla \psi| - \frac{\nabla T \cdot \nabla \psi}{|\nabla \psi|} \nabla \psi, \quad (19)$$

with all terms being evaluated at the cell faces due to the staggered grid layout.

III. RESULTS

A. Thermocapillary migration of a drop in the limit of zero Marangoni number

Consider a spherical drop of radius r_0 of one fluid initially at rest in another fluid, both fluids having the same thermal diffusivity. The flow field is subjected to a time-invariant linear temperature profile, i.e., thermal conductivity is infinite and hence the Marangoni number is $\text{Ma}=0$. The purpose of this test case is to study the stability and accuracy of the finite-volume balanced-force implementation of the Marangoni stress. In the limit of zero Marangoni number and small Reynolds number, Young, Goldstein, and Block¹ (YGB) calculated the steady state velocity of a neutrally buoyant drop (sphere) in a constant temperature gradient field in an infinite unbounded domain for two fluids of equal thermal conductivity to be

$$v_{\text{YGB}} = - \frac{2\sigma_T G_T r_0}{6\mu_b + 9\mu_d}. \quad (20)$$

In our computational model, a drop of radius $r_0=0.5$ is placed inside a box of size $10r_0 \times 10r_0 \times 15r_0$, with the drop's center at the box centerline and $3r_0$ above the bottom

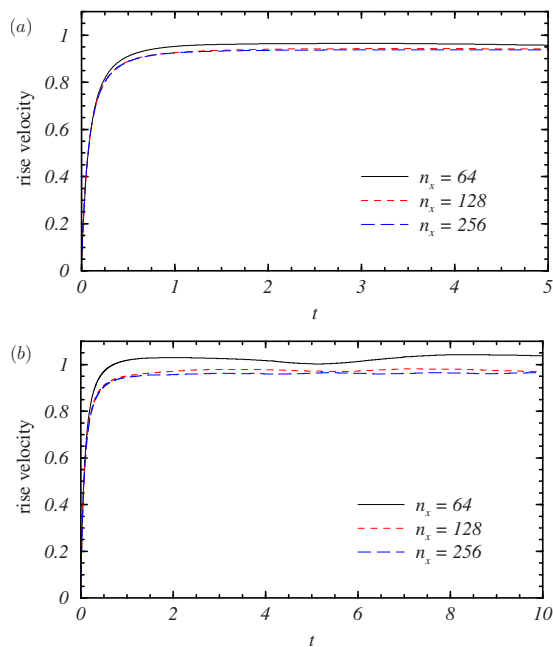


FIG. 1. (Color online) Normalized rise velocity in the limit of vanishing Reynolds and Marangoni numbers for (a) the three-dimensional rectangular box case and (b) the axisymmetric case for various grid sizes n_x as indicated.

wall. No-slip boundary conditions are imposed on the top and bottom walls, and periodic boundary conditions are used in the horizontal directions. A linear temperature field is imposed in the vertical direction, with $T=0$ on the bottom wall and $T=1$ on the top wall, resulting in $G_T=0.13$. The fluid properties are $\rho_d=\rho_b=0.2$, $\mu_b=\mu_d=0.1$, $T_0=0$, $\sigma_0=0.1$, and $\sigma_T=-0.1$. Using these values, the theoretical rise velocity of a spherical drop is $v_{YGB}=8.888\bar{8}\times 10^{-3}$. In the simulations, the rise velocity v_r is calculated from

$$v_r = \frac{\int_V \psi v dV}{\int_V \psi dV} = \frac{\sum_{cv} \psi_{cv} v}{\sum_{cv} \psi_{cv}}, \quad (21)$$

where v is the vertical component of the velocity vector evaluated at the control volume centroid.

Figure 1 shows the temporal evolution of the numerically calculated rise velocity normalized by v_{YGB} using the RLSG method with equal resolution flow solver and G -grids corresponding to $n_x=64$, 128, and 256 nodes per box width. The RLSG method exhibits decreasing oscillation amplitudes with increasing grid resolutions and converges to an asymptotic value of $v_r/v_{YGB}\approx 0.94$ in the full three-dimensional case and to $v_r/v_{YGB}\approx 0.96$ in the axisymmetric case. These are comparable to the value of 0.97 reported in Ref. 24. For the axisymmetric drop, it was necessary to change the horizontal wall boundary condition to slip rather than periodic; both of these artificial boundary conditions are employed in order to reduce the effects of the finite geometry in comparing with the unbounded theoretical results of YGB.¹ The slower rise velocities in the finite simulations compared with the theoretical value determined in the unbounded idealized problem are probably due to confinement effects, i.e., the difference between a finite domain with periodic boundary conditions and the infinite domain in the

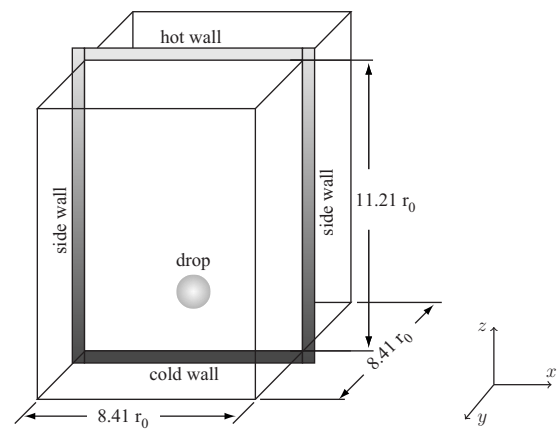


FIG. 2. Schematic of the test cell.

theoretical approximation, resulting in differences of about 5% (similar conclusions have been made for the impact of finite domains on solid particles²⁵). The differences between the three-dimensional and axisymmetric results are also probably due to confinement effects, i.e., the difference between a rectangular box with periodic boundary conditions and a cylindrical sheet with slip boundary conditions, resulting in differences of about 2%.

In summary, the proposed method to include the Marangoni force into a balanced-force finite-volume fluid solver using the RLSG front tracking approach yields stable results, comparable in accuracy to previously reported numerical results for axisymmetric flows.

B. Thermocapillary migration of a drop with finite Marangoni number

These simulations consist of calculating the thermocapillary motion of an axisymmetric drop and a fully three-dimensional drop using fluids of finite Marangoni numbers. Due to the finite Marangoni numbers, there is a two-way coupling between the temperature equation and the Navier–Stokes equations. This is expected to result in a reduction of the tangential temperature gradients at the drop interface due to the interfacial flow driven by the Marangoni stress, which in turn will also be reduced. The aim here is to reproduce conditions corresponding to reduced-gravity experiments.^{13,14}

Figure 2 shows a schematic of the test cell used in the

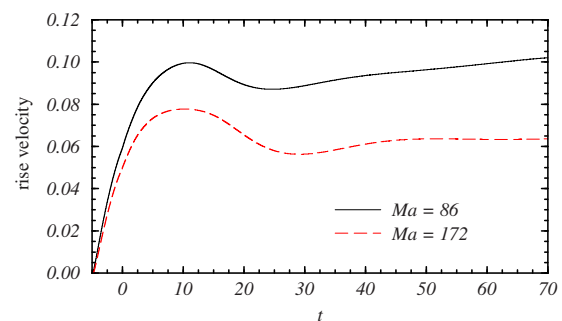


FIG. 3. (Color online) Axisymmetric drop rise velocity for $Re=17.79$ and Ma as indicated.

TABLE I. Grid convergence for peak rise velocity of axisymmetric drop.

Points per r_0	Ma	Peak rise velocity	Error
11.41	86	0.096 25	1.134×10^{-4}
22.83	86	0.096 68	1.022×10^{-4}
45.65	86	0.098 47	5.475×10^{-5}
91.31	86	0.099 67	2.317×10^{-5}
182.61	86	0.100 55	...
11.41	172	0.076 68	5.102×10^{-5}
22.83	172	0.075 55	8.095×10^{-5}
45.65	172	0.076 32	6.076×10^{-5}
91.31	172	0.077 74	2.316×10^{-5}
182.61	172	0.078 62	...

microgravity experiments.^{13,14} It consists of a 60 mm \times 45 mm \times 45 mm rectangular box of no-slip walls. The bottom cold wall is held at a constant $T_0=283$ K, the top hot wall is held at a constant $T_1=343$ K, and the side walls are held at a time-invariant linear temperature profile from T_0 at the bottom to T_1 at the top. At time $t=-1$ s, a circular drop of radius $r_0=5.35$ mm of Fluorinert FC-75 is inserted into a bulk liquid of silicone oil (DOW-Corning DC-200 series of nominal viscosity 10 cS). The drop's initial center is 15 mm from the bottom. The temperature of the drop is set to the bulk fluid temperature at the drop center. Although this is a departure from the classical initial condition of a linear temperature distribution inside the drop, this is likely a better approximation of the experiment.²⁶ At $t=0$ s the drop is released. Between the insertion and release times, the drop is held in place while the temperature and velocity fields in the fluids are allowed to develop.

For the surface tension between silicone oil and Fluorinert,^{14,27} we use $\sigma_0=0.007$ N/m and $\sigma_T=-3.6 \times 10^{-5}$ N/m K. The density variation with temperature of the two liquids is assumed to be of the form

$$\rho = A + BT, \quad (22)$$

where for the silicone oil $A=1200$ kg/m³ and $B=-0.9$ kg/K m³ and for the Fluorinert $A=2504$ kg/m³ and $B=-2.48$ kg/K m³, and the viscosity variation with temperature of the two liquids is assumed to be of the form

$$\mu = \exp(C + D/T), \quad (23)$$

where for the silicone oil $C=-10.17$ and $D=1643$ and for the Fluorinert $C=-11.76$ and $D=1540$.^{13,14} The thermal conductivity and the heat capacity of the silicone oil are set to a constant $k=0.133$ 89 W/mK and $c_p=1778.2$ J/kg K, and those of the Fluorinert are $k=0.063$ W/mK and $c_p=1047.0$ J/kg K. Using the above values and relations with a reference temperature of $T=313$ K (evaluated at the test cell center), the reference values of the analyzed case are $Re=17.79$, $Ma=1723$, and $Ca=0.0275$. Note that the relatively high Marangoni number results in very thin thermal boundary layers (they scale as $Ma^{-0.5}$) that are challenging to resolve. For that reason, we consider two larger thermal conductivities in order to increase the thermal boundary layer thickness, corresponding to $Ma=86$ and 172.

Figure 3 shows the rise velocity as a function of time for $Ma=86$ and 172. In both cases, there is an initial overshoot followed by a quasisteady rise velocity. This initial transient behavior has also been observed in other numerical simulations.¹⁵ Comparing the two Ma cases, there is a decrease in the overshoot and the quasisteady rise velocity with increasing Ma , consistent with transient simulations of non-

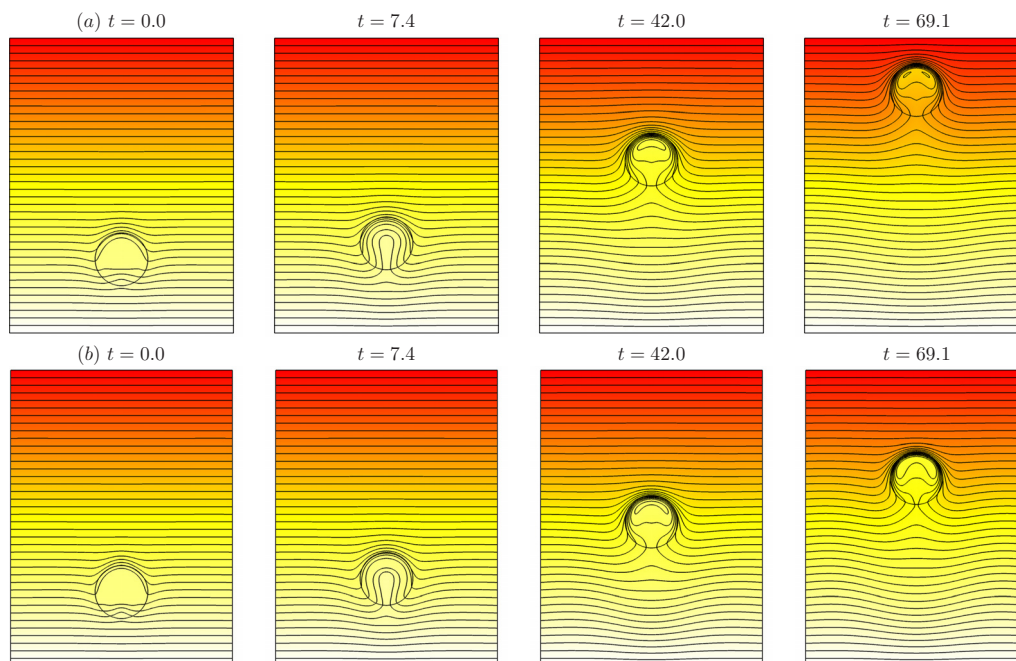


FIG. 4. (Color online) Isotherms for axisymmetric simulations with (a) $Ma=86$ and (b) $Ma=172$ at indicated times; animations of the drop rise are available with the online version. The temperature at the bottom of the container is $T=0.904$ (white) and at the top it is $T=1.096$ (red online); contours are drawn in intervals of $\Delta T=0.005$ (enhanced online). [URL: <http://dx.doi.org/10.1063/1.3529442.1>][URL: <http://dx.doi.org/10.1063/1.3529442.2>]

deformable drops.¹⁵ The peak rise velocities are of the same order as those reported in the experiments of Ref. 13, where a “knee” structure in the migration velocity history, similar to that found in our own simulations in Fig. 3, was reported.

Table I summarizes the results of a grid convergence study, showing first-order convergence of the error between the two finest grids. To determine the error, the solution from the finest grid is used as the “exact” solution.

Isotherm plots for $Ma=86$ and 172 are shown in Fig. 4; the online version of the paper includes movies of the evolutions. These provide an explanation for the observed rise velocity dependence on Ma . Initially, the drop is subjected to a large temperature gradient at its surface, resulting in strong Marangoni forces and a strong induced flow field. This in turn results in the initial peak in rise velocity. The strong Marangoni force-induced velocities then lead to a partial homogenization of the temperature at the drop surface, thus reducing the Marangoni force and hence the rise velocity until a quasisteady state is reached. In the $Ma=86$ case, the temperature field is only slightly disturbed except for the local regions surrounding the drop. The relatively benign isotherms inside and outside the drop help maintain a significant temperature gradient at the phase interface, resulting in the relatively high rise velocity. The homogenization is more pronounced at the larger Marangoni number, as is the disruption of the temperature field.

1. Initial conditions

The exact experimental initial conditions are often difficult or impossible to determine. In particular, there is considerable uncertainty in the initial temperature distribution in the drop prior to its release. In the experiments, the drop is introduced into the box via a syringe drawing liquid from a reservoir presumably held at a constant temperature. If after introduction, the drop is held by the syringe tip for an extended period of time to let the velocities generated by the introduction of the drop decay and to allow the drop’s temperature to adjust to the bulk temperature distribution, Marangoni forces will induce significant flow both in the drop and the bulk. If, on the other hand, the drop is quickly released, the temperature distribution inside the drop does not have sufficient time to adjust. This leaves the exact initial temperature distribution inside the drop unknown. In addition, the injector syringe itself is not small compared to the drop radius, and detaching it from the drop may lead to deformations of the initial drop shape that are not documented in the available experimental data (the protocol in the microgravity experiments was to begin recording data some time after the drop was released).

To study the impact of the uncertainty in the initial temperature distribution within the drop, we consider four different axisymmetric cases at $Ma=86$ and $Ma=172$. In the first two cases, the temperature within the drop is assumed to be isothermal and the drop is either immediately released or held for 4.9 time units. In the other two cases, the initial temperature distribution within the drop is assumed to match the linear profile in the bulk phase and the drop is released either immediately or after being held for 4.9 time units.

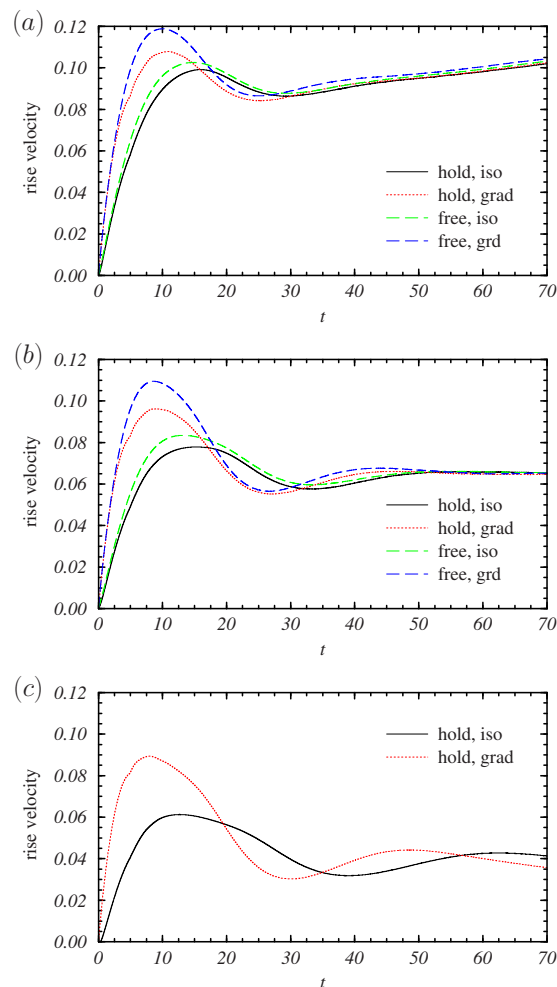


FIG. 5. (Color online) Axisymmetric drop rise velocity for different initial conditions with $Re=17.79$ and (a) $Ma=86$, (b) $Ma=172$, and (c) $Ma=345$. The initially isothermal drop is released at $t=4.9$ (hold, iso) and at $t=0$ (free, iso). The drop with an initial temperature gradient that matches the surrounding bulk phase temperature distribution is released at $t=4.9$ (hold, grad) and at $t=0$ (free, grad).

Figure 5 shows the rise velocity as a function of time for four different initial conditions and indicated Ma . Significant differences can be seen in the initial transients. Imposing an initial linear temperature profile results in a much larger initial overshoot in rise velocity compared to imposing a constant initial temperature within the drop. On the other hand, holding the drop in place prior to release for 4.9 time units reduces the overshoot in both cases. After the initial overshoot, the rise velocity settles to a quasisteady positive value which is very similar in all four cases. In the $Ma=172$ case, the difference between the initial peak rise velocities is far more pronounced than in the $Ma=86$ case. Also, in the $Ma=86$ case, the rise velocities settle to a quasisteady state after about 30 time units. This does not happen in the $Ma=172$ case until 50 time units have passed and the drop has traveled through 50% of the apparatus. Further increasing the Marangoni number to $Ma=345$ results in extending the time to quasisteady state beyond 75 time units by which time the drop has again traveled through 50% of the apparatus. By increasing the Marangoni number, we are decreasing the thermal conductivity. This increases the time scale asso-

TABLE II. Grid convergence for peak rise velocity of three-dimensional drop.

Points per r_0	Peak rise velocity	Error
5.71	0.097 17	8.495×10^{-5}
11.41	0.095 89	1.186×10^{-4}
22.83	0.098 15	5.904×10^{-5}
45.65	0.100 39	...

ciated with the thermal diffusivity. The larger diffusive time scale ensures that the impact of the differing initial conditions will not rapidly diffuse away to yield similar quasi-steady rise velocities. Thus, in the experiments which are performed with large Marangoni numbers and limited run time, the drop rise velocity history is dominated by transient behavior.¹³ In summary, the simulation results indicate that the initial condition for the temperature distribution within the drop as well as the initial holding time has a significant impact on the initial transient and subsequent evolution.

2. Domain geometry

Most numerical simulations of thermocapillary migration are axisymmetric, whereas the experimental apparatus is a three-dimensional box. Here we examine the impact that the axisymmetric simplification has on the rise velocity. To this end, fully three-dimensional simulations were performed with $Ma=86$. Table II summarizes the results of a grid convergence study in the three-dimensional case, showing again first-order convergence of the error between the two finest grids, using the finest grid resolution as the exact solution to calculate the error. In these simulations, we use the initial and boundary conditions described in the beginning of Sec. III B (i.e., no-slip walls and Dirichlet temperature boundaries with an initially isothermal drop held in place for 4.9 time units).

Figure 6 shows the isotherms for the three-dimensional simulations; the online version of the paper includes a movie of the evolution. The vertical plane shown in this figure cuts through the center of the box and is parallel to the x-y plane. While these isotherms look very similar to the axisymmetric case, the imprint of the three-dimensional geometry can be seen in the snapshots of the vorticity in a horizontal plane

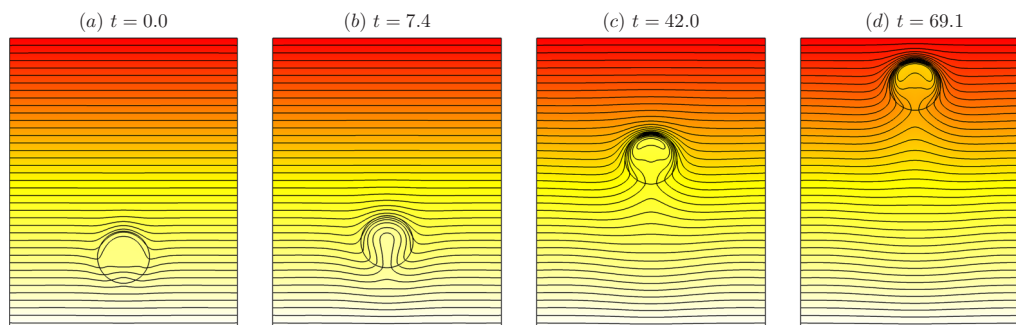


FIG. 6. (Color online) Isotherms for three-dimensional simulation with $Ma=86$ at indicated times; an animation of the drop rise is available with the online version. The bottom (white) and top (red online) are at respective temperatures of $T=0.904$ and $T=1.096$ with a temperature change between contours of $\Delta T=0.005$ (enhanced online). [URL: <http://dx.doi.org/10.1063/1.3529442.3>]

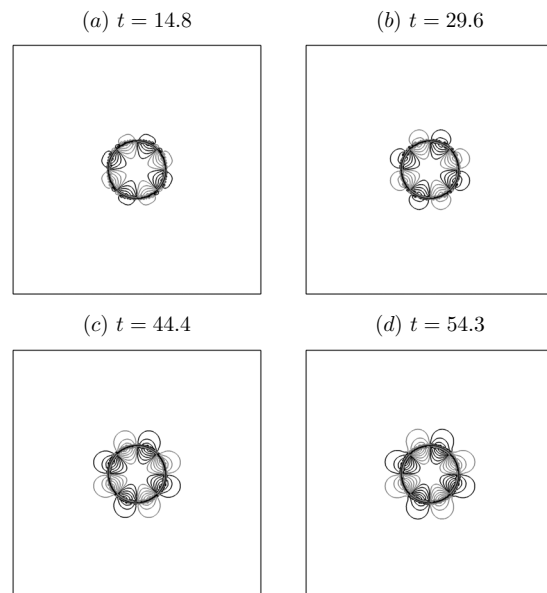


FIG. 7. Vorticity (z -component) contours plotted with quadratic spacing for the three-dimensional simulation with $Ma=86$ at indicated times. Maximum and minimum contour values are 1.5 and -1.5 , respectively. Positive vorticity (out of the page) is black, negative vorticity (into the page) is gray.

through the center of drop shown in Fig. 7. The component of vorticity perpendicular to the page is shown in this figure. In an axisymmetric simulation, this component would be zero. The pattern of positive and negative vorticity is aligned with the wall corners.

The impact of domain geometry can also be observed in a comparison of the three-dimensional and axisymmetric runs with varying cross-sectional areas, as shown in Fig. 8. Observe that for the case when the axisymmetric and three-dimensional cross-sectional areas are equal, the rise velocity in the three-dimensional box is noticeably higher. This is most likely due to the geometry of the box, which reduces the blockage effects that are felt in the axisymmetric simulations. Decreasing the cylindrical cross-sectional area to 0.5 with respect to the box has no impact as the diameter of the cylinder is still sufficiently large compared to the drop radius. Further reductions in the cylindrical cross-sectional area result in large decreases in migration velocities. The impact of the blockage effects is shown in Fig. 9, which

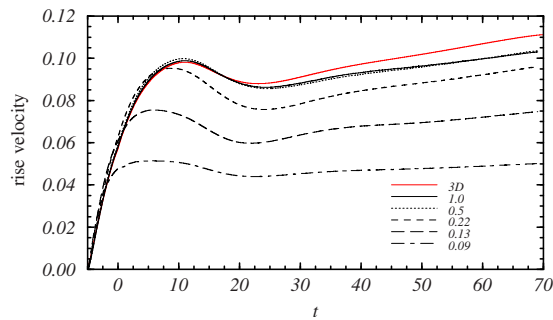


FIG. 8. (Color online) Rise velocity history of the three-dimensional drop [solid gray (solid red)] compared with axisymmetric simulations with ratios of cross-sectional area to that of the box as indicated.

compares the percent deformation as a function of zenith angle for several cylindrical cross-sectional area ratios. As can be seen, the magnitude of the deformation increases as cross-sectional area is decreased. The impact of the blockage effects can also be seen in Fig. 10 which compares the vorticity contours for four axisymmetric simulations with different cross-sectional areas. It can be seen that the structure of the vorticity undergoes a minimal change inside the drop. Outside the drop, the vorticity structure undergoes a significant deformation due to the interaction of the wall and drop. The impact of these blockage effects increases over time. The difference in blockage effects between the domains occurs because the distance between the wall and the drop varies with azimuthal location in the three-dimensional box, but is constant in axisymmetric simulations. There is currently no *a priori* way of determining the appropriate cross-sectional area ratio such that the cylindrical boundaries will mimic the effect of the box boundaries. This suggests that axisymmetric simulations will not be able to reproduce the rise velocity observed experimentally in rectangular boxes.

The impact of domain geometry can also be seen in the azimuthal drop deformations which have typically been ignored in thermocapillary migration simulations. Figure 11 shows contours of the percent deformation away from spherical of the three-dimensional drop surface as a function of the azimuthal and zenith angles for the indicated time. Mode 4 deformations corresponding to the azimuthal location of the walls are evident at both times and appear at different zenith angles. These deformations persist at ap-

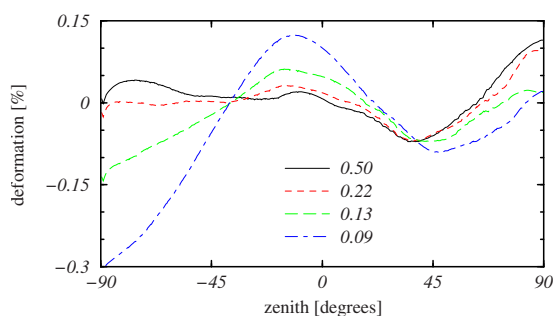


FIG. 9. (Color online) Axisymmetric drop deformation with cross-sectional area relative to that of the box as indicated. The “north pole” of the drop corresponds to a zenith angle of 90° , and the “south pole” corresponds to -90° .

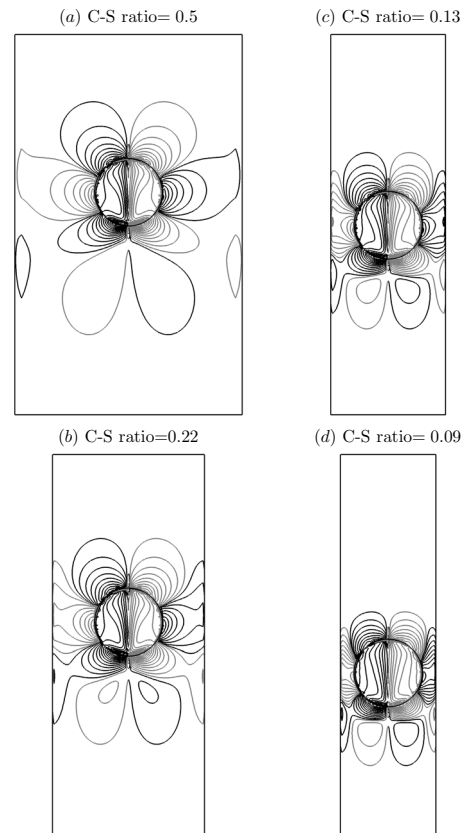


FIG. 10. Azimuthal vorticity contours plotted with quadratic spacing for the axisymmetric simulations with indicated cross-sectional area ratio and $Ma=86$ at time $t=42.0$. Maximum and minimum contour values are 4.0 and -4.0 , respectively. Positive vorticity (out of the page) is black, negative vorticity (into the page) is gray.

proximately the same level under grid refinement, which suggests that they are the imprint of the box and not a numerically induced deformation.

Figure 12 shows plots of the percentage axisymmetric deformation away from spherical of the axisymmetric drop at four different times for $Ma=86$ and 172. The deformation of the drop changes rapidly immediately following its release. This is due to the large temperature gradients at the drop surface leading to large Marangoni forces. The magnitude of the deformations is small and is similar to those of the three-dimensional drop. Although these deformations are small, it is argued in Ref. 5 that the deformations significantly influence the temperature distribution along the drop surface and thus impact the drop migration behavior. The authors of Ref. 5 investigate three-dimensional drop migration with Marangoni numbers up to $Ma=50$ and also observe deformations which are nonaxisymmetric. Two snapshots of the variation in the tangential temperature gradient along the drop interface for three different zenith angles are shown in Fig. 13. The imprint of domain geometry can be seen. The significant variation in the temperature gradient which grows over time may also explain the difference in drop rise behavior between the three-dimensional and axisymmetric cases.

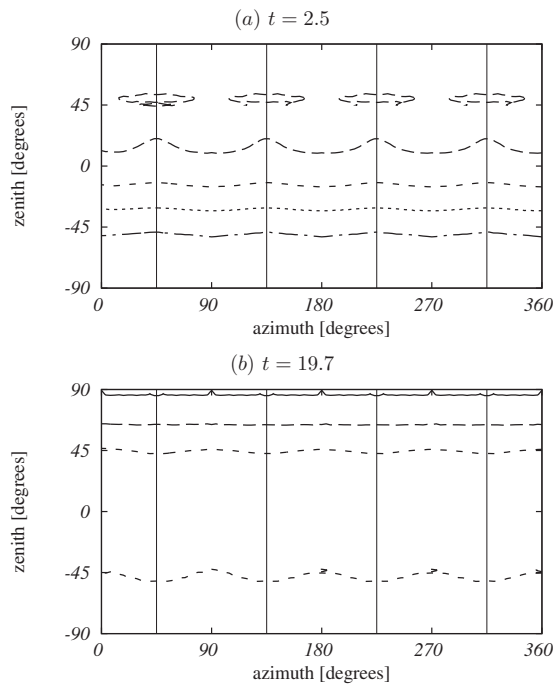


FIG. 11. Contours of the percent deformation of the three-dimensional drop away from spherical at two times. The contour values are 0.1% (solid line), 0.5% (long dashes), 0.0% (short dashes), -0.05% (dots), and -0.1% (dashed-dot). The north pole of the drop corresponds to a zenith angle of 90° and the south pole corresponds to -90° . The solid vertical lines indicate the azimuthal locations of the box corners.

3. Fluid properties

Often, the assumption of temperature-independent densities and viscosities is made in thermocapillary motion simulations. In the experiment, the change in densities for the given temperature range of the drop and bulk fluids is

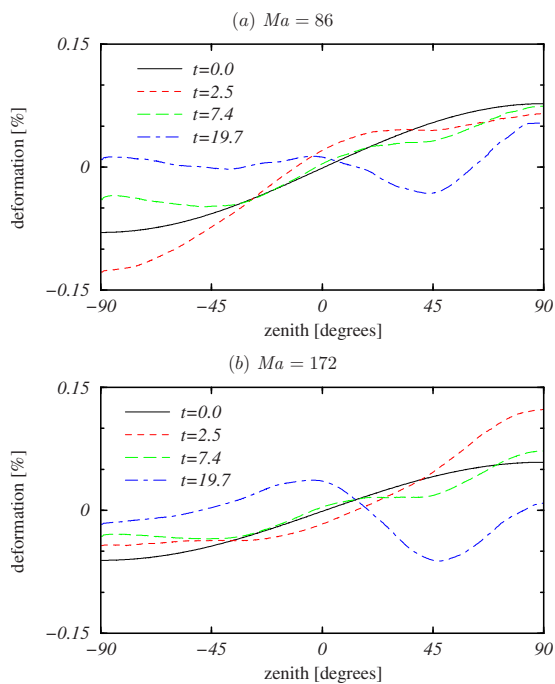


FIG. 12. (Color online) Axisymmetric drop deformation at various times for $Re=17.79$ and Ma as indicated.

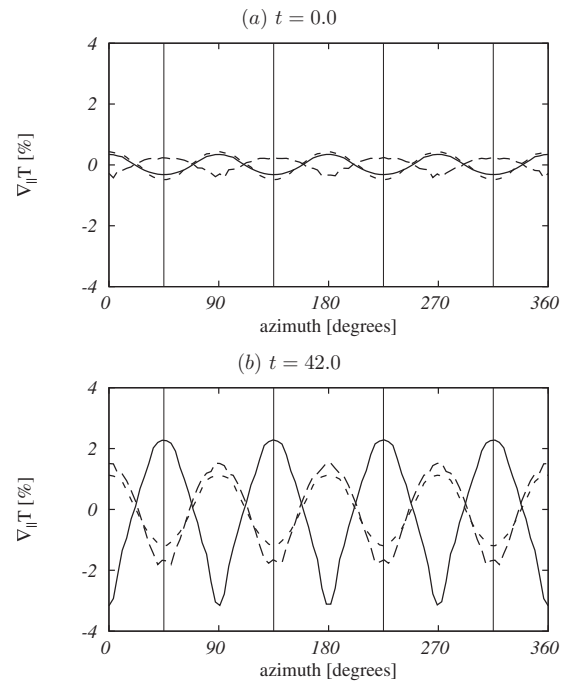


FIG. 13. Percent variation of temperature gradient along the surface of the drop as a function of azimuthal angle for the indicated times with zenith angles of 0° (solid line), -30° (long dashes), and -60° (short dashes). The solid vertical lines indicate the azimuthal locations of the box corners.

8.6% and 5.8%, respectively. The change in viscosities for the given temperature range of the drop and bulk fluids is 103.4% and 111.3%, respectively. Figure 14 shows the rise velocity as a function of time when density and viscosity are

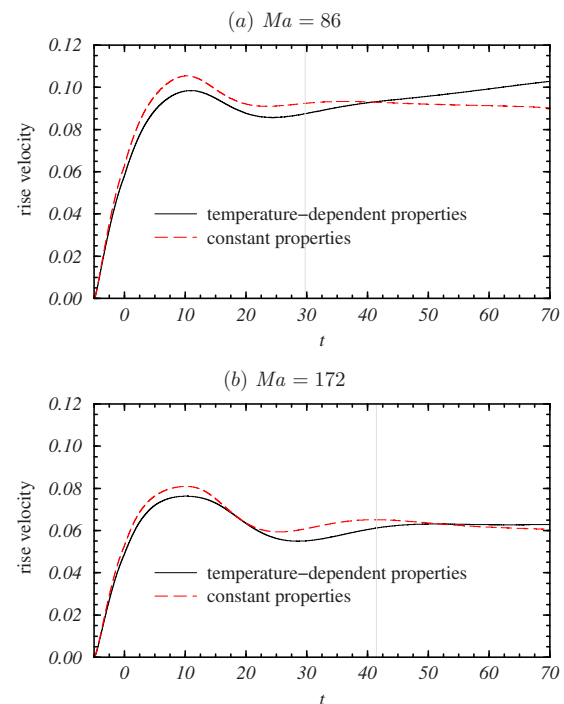


FIG. 14. (Color online) Axisymmetric drop rise velocity for $Re=17.79$ and Ma as indicated with temperature-dependent densities and viscosities (solid line) and constant densities and viscosities (dashed line). The vertical lines indicate the time at which the drop crossed the center plane of the box.

treated as a function of temperature and when they are held constant. The vertical line indicates the time at which the center of the drop crosses the center of the box. The discrepancy between the migration velocities can be explained in terms of the drag forces acting on the drop. For the case of constant temperature material properties, the density and viscosity are computed based on the temperature at the center of the box. We consider this our base case and compare it to the case where the material properties are allowed to vary with temperature. In the latter, when the drop is below the midplane of the box, it “sees” a fluid density and viscosity based on a lower temperature compared to the base case. This results in a larger drag force on the drop which leads to a smaller migration velocity before the drop passes through the box center. Above the midplane, the situation reverses and the drop with variable temperature properties gains speed due to the decrease in drag while the drop in the base case slows down due to the increase in drag. The assumption of constant density and viscosity is not valid in this experiment.

IV. CONCLUSION

Four of the open questions regarding thermocapillary migration of drops have been addressed. The initial conditions of the drop are not all that important for the quasisteady behavior of the drop in low Marangoni number regimes. For larger Marangoni numbers, the time to quasisteady state is significant compared to the duration of the experiment. The distance traveled by the drop during this time is also significant compared to the size of the experimental apparatus. Thus, for larger Marangoni numbers details of the initial conditions dominate the drop behavior. This was seen by examining the rise velocity history of the drop with four different initial conditions for $Ma=86, 172, \text{ and } 345$. Domain geometry (three-dimensional versus axisymmetric) is also an important consideration and impacts the quasisteady behavior of the drop as evidenced by the difference in rise velocity for three-dimensional and axisymmetric simulations. The non-axisymmetric deformations and temperature distributions which develop play a significant role in drop migration. These effects coupled with the difficulty of choosing an appropriate cylindrical cross-sectional area to match the three-dimensional blockage effects make it very unlikely that axisymmetric simulations will be able to match the drop behavior from experiments performed in rectangular boxes. To make numerical simulations of thermocapillary migration experiments feasible, the experiments should be performed in a cylinder as opposed to a box as axisymmetric simulations are orders of magnitude cheaper than full three-dimensional simulations. The deformations of the drop are very small; however, they influence the temperature distribution and impact the migration velocity in an appreciable way. The deformations away from axisymmetric in the regimes we have investigated are due to the geometry of the box. We have not found any evidence of spontaneous breaking of axisymmetry due to flow instabilities. The influence of the variation of density and viscosity with temperature was non-trivial and should be included in numerical models.

ACKNOWLEDGMENTS

This work was supported by the National Science Foundation grants (Contract Nos. DMS-0808045, DMS-0922864, and TG-DMS090031) and the Korean Science and Engineering Foundation WCU grant (Contract No. R32-2009-000-20021-0). Computations were performed using the ASU Ful-ton High Performance Computing Initiative and the NSF Teragrid Ranger cluster.

- ¹N. O. Young, J. S. Goldstein, and M. J. Block, “The motion of bubbles in a vertical temperature gradient,” *J. Fluid Mech.* **6**, 350 (1959).
- ²R. S. Subramanian, “The motion of bubbles and drops in reduced gravity,” in *Transport Processes in Drops, Bubbles, and Particles*, edited by R. D. Chhabra and D. Dekee (Hemisphere, New York, 1992), p. 1.
- ³R. S. Subramanian, R. Balasubramaniam, and G. Wozniak, “Fluid mechanics of bubbles and drops,” in *Physics of Fluids in Microgravity*, edited by R. Monti (Taylor & Francis, London, 2002), p. 149.
- ⁴J. C. Chen and Y. T. Lee, “Effect of surface deformation on thermocapillary bubble migration,” *AIAA J.* **30**, 993 (1992).
- ⁵H. Haj-Hariri, Q. Shi, and A. Borhan, “Thermocapillary motion of deformable drops at finite Reynolds and Marangoni numbers,” *Phys. Fluids* **9**, 845 (1997).
- ⁶R. Balasubramaniam and A.-T. Chai, “Thermocapillary migration of droplets: An exact solution for small Marangoni numbers,” *J. Colloid Interface Sci.* **119**, 531 (1987).
- ⁷S. W. J. Welch, “Transient thermocapillary migration of deformable bubbles,” *J. Colloid Interface Sci.* **208**, 500 (1998).
- ⁸A. Acrivos, D. J. Jeffrey, and D. A. Saville, “Particle migration in suspensions by thermocapillary or electrophoretic motion,” *J. Fluid Mech.* **212**, 95 (1990).
- ⁹S. Nas and G. Tryggvason, “Thermocapillary interaction of two bubbles or drops,” *Int. J. Multiphase Flow* **29**, 1117 (2003).
- ¹⁰S. Nas, M. Muradoglu, and G. Tryggvason, “Pattern formation of drops in thermocapillary migration,” *Int. J. Heat Mass Transfer* **49**, 2265 (2006).
- ¹¹R. Borcia and M. Bestehorn, “Phase-field simulations for drops and bubbles,” *Phys. Rev. E* **75**, 056309 (2007).
- ¹²M. Treuner, V. Galindo, G. Gerbeth, D. Langbein, and H. J. Rath, “Thermocapillary bubble migration at high Reynolds and Marangoni numbers under low gravity,” *J. Colloid Interface Sci.* **179**, 114 (1996).
- ¹³P. H. Hadland, R. Balasubramaniam, G. Wozniak, and R. S. Subramanian, “Thermocapillary migration of bubbles and drops at moderate to large Marangoni number and moderate Reynolds number in reduced gravity,” *Exp. Fluids* **26**, 240 (1999).
- ¹⁴G. Wozniak, R. Balasubramaniam, P. H. Hadland, and R. S. Subramanian, “Temperature fields in a liquid due to the thermocapillary motion of bubbles and drops,” *Exp. Fluids* **31**, 84 (2001).
- ¹⁵Z. Yin, P. Gao, W. Hu, and L. Chang, “Thermocapillary migration of nondeformable drops,” *Phys. Fluids* **20**, 082101 (2008).
- ¹⁶L. D. Landau and E. M. Lifshitz, *Fluid Mechanics* (Pergamon, New York, 1959).
- ¹⁷M. Herrmann, “A balanced force refined level set grid method for two-phase flows on unstructured flow solver grids,” *J. Comput. Phys.* **227**, 2674 (2008).
- ¹⁸G.-S. Jiang and D. Peng, “Weighted ENO schemes for Hamilton-Jacobi equations,” *SIAM J. Sci. Comput. (USA)* **21**, 2126 (2000).
- ¹⁹C. W. Shu, “Total-variation-diminishing time discretization,” *SIAM (Soc. Ind. Appl. Math.) J. Sci. Stat. Comput.* **9**, 1073 (1988).
- ²⁰O. Desjardins, G. Blanquart, G. Balarac, and H. Pitsch, “High order conservative finite difference scheme for variable density low Mach number turbulent flows,” *J. Comput. Phys.* **227**, 7125 (2008).
- ²¹M. Herrmann, G. Blanquart, and V. Raman, “Flux corrected finite volume scheme for preserving scalar boundedness in reacting large-eddy simulations,” *AIAA J.* **44**, 2879 (2006).
- ²²S. P. van der Pijl, A. Segal, and C. Vuik, “A mass-conserving level-set method for modelling of multi-phase flows,” *Int. J. Numer. Methods Fluids* **47**, 339 (2005).

- ²³J. U. Brackbill, D. B. Kothe, and C. Zemach, "A continuum method for modeling surface tension," *J. Comput. Phys.* **100**, 335 (1992).
- ²⁴M. Muradoglu and G. Tryggvason, "A front-tracking method for computation of interfacial flows with soluble surfactants," *J. Comput. Phys.* **227**, 2238 (2008).
- ²⁵J. Happel and H. Brenner, *Low Reynolds Number Hydrodynamics* (Martinus Nijhoff, The Hague, 1983).
- ²⁶R. S. Subramanian (private communication).
- ²⁷S. Someya and T. Munakata, "Measurement of the interface tension of immiscible liquids interface," *J. Cryst. Growth* **275**, e343 (2005).